A *Tmc1* mutation reduces calcium permeability and expression of mechanoelectrical transduction channels in cochlear hair cells

Maryline Beurg[a], Amanda Barlow[a], David N. Furness[b], and Robert Fettiplace[a,1]

[a]Department of Neuroscience, University of Wisconsin School of Medicine and Public Health, Madison, WI 53706; and [b]School of Life Sciences, Keele University, Keele, ST5 5BG Staffordshire, United Kingdom

Edited by Ulrich Müller, Johns Hopkins University, Baltimore, MD, and accepted by Editorial Board Member Jeremy Nathans August 31, 2019 (received for review May 9, 2019)

Mechanoelectrical transducer (MET) currents were recorded from cochlear hair cells in mice with mutations of transmembrane channel-like protein TMC1 to study the effects on MET channel properties. We characterized a *Tmc1* mouse with a single-amino-acid mutation (D569N), homologous to a dominant human deafness mutation. Measurements were made in both *Tmc2* wild-type and *Tmc2* knockout mice. By 30 d, *Tmc1* pD569N heterozygote mice were profoundly deaf, and there was substantial loss of outer hair cells (OHCs). MET current in OHCs of *Tmc1* pD569N mutants developed over the first neonatal week to attain a maximum amplitude one-third the size of that in *Tmc1* wild-type mice, similar at apex and base, and lacking the tonotopic size gradient seen in wild type. The MET-channel Ca^{2+} permeability was reduced 3-fold in *Tmc1* pD569N homozygotes, intermediate deficits being seen in heterozygotes. Reduced Ca^{2+} permeability resembled that of the *Tmc1 p*M412K *Beethoven* mutant, a previously studied semidominant mouse mutation. The MET channel unitary conductance, assayed by single-channel recordings and by measurements of current noise, was unaffected in mutant apical OHCs. We show that, in contrast to the *Tmc1* M412K mutant, there was reduced expression of the TMC1 D569N channel at the transduction site assessed by immunolabeling, despite the persistence of tip links. The reduction in MET channel Ca^{2+} permeability seen in both mutants may be the proximate cause of hair-cell apoptosis, but changes in bundle shape and protein expression in *Tmc1* D569N suggest another role for TMC1 apart from forming the channel.

cochlea | hair cell | deafness | mechanotransducer channel | transmembrane channel-like protein

Sound stimuli are converted into electrical signals by the opening of mechanoelectrical transducer (MET) channels in the stereocilia projecting from the top of each hair cell. The MET channels are thought to be located at the lower ends of extracellular tip links connecting adjacent stereocilia (1–3). These channels are cation channels with high permeability to Ca^{2+} (4–6). There has been much controversy over the molecular underpinning of the channel, but the current view is that the transmembrane channel-like protein isoforms 1 and 2 (TMC1 and TMC2) play a pivotal role in MET channel function (7, 8). Both TMC isoforms have been localized to the site of the MET channels at the tips of the shorter stereocilia (9), and mutation in either alters ion conduction through the channels (10–12). TMC2 is expressed early in postnatal development of the mouse cochlea and is replaced by TMC1 by the end of the first postnatal week (8, 13). *Tmc1* knockout mice lack MET currents in outer hair cells (OHCs) after postnatal day (P)8 and are deaf (8, 10). However, TMC1 may not be the sole member of the MET channel: other components proposed to interact with TMC1 at the transduction site include LHFPL5 (14, 15), TMIE (16, 17), and CIB2 (18).

Neither the configuration nor the role of TMC family members has been clear because of past inability to express the protein in a heterologous system and have it transported to the plasma membrane (19). However, a recent success was reported, but without production of mechanosensitivity (20). Some insight was derived from a possible evolutionary relationship between TMC1 and TMEM16 (ANO1), a Ca^{2+}-activated chloride channel (21, 22). Modeling based on homology between TMC1 and TMEM16A proposed dimeric TMC1 channels, each component having 10 transmembrane domains, with an ion-conducting cavity generated by transmembrane domains 4 to 7 (23, 24). According to this modeling, the ion-conducting cavity of a hypothetical TMC1 channel contains several critical residues the mutations of which are linked to human genetic deafness. These mutations include D572N (7), D572H (25), M418K (26), and G417R (27). All mutations are associated with dominant deafness DFNA36 and substitute a positively charged residue (lysine or arginine) or remove a negatively charged residue (aspartate), which may influence Ca^{2+} binding within the channel pore. We shall focus on the properties of the mouse mutation *Tmc1* p.D569N (25) and compare it with *Tmc1* p.M412K, known as *Beethoven* (11, 12, 28, 29), these being the sites in the mouse TMC1 homologous to the D572 and M418 human mutations. Both are semidominant mutations linked to progressive hearing loss, but they have subtly different effects on MET channel properties.

Materials and Methods

Mouse Mutants. The care and use of animals for all experiments described conformed to NIH guidelines and were approved by the Institutional Animal Care and Use Committee at the University of Wisconsin, Madison. The *Tmc2*

Significance

Cochlear hair cells transduce sound into electrical signals by activation of mechanically sensitive ion channels thought to be formed by TMC1. We generated a single aspartate/asparagine substitution in mouse TMC1 which is homologous to a human genetic deafness mutation. The main consequence was reduction in the Ca^{2+} permeability of the mechanically sensitive channel with little change in its unitary conductance. Nevertheless, there was a much reduced expression of the ion channel, which led within 4 wk to death of the outer hair cells culminating in deafness. The mouse mutant accounts for the human deafness and implies that TMC1, in addition to forming the mechanically sensitive ion channel, regulates its own expression.

Author contributions: M.B. and R.F. designed research; M.B., A.B., D.N.F., and R.F. performed research; M.B., A.B., and R.F. analyzed data; and M.B. and R.F. wrote the paper.

The authors declare no conflict of interest.

This article is a PNAS Direct Submission. U.M. is a guest editor invited by the Editorial Board.

[1]To whom correspondence may be addressed. Email: fettiplace@wisc.edu.

This article contains supporting information online at www.pnas.org/lookup/suppl/doi:10.1073/pnas.1908058116/-/DCSupplemental.

First published September 23, 2019.

knockout (B6.129S5-*Tmc2*^{tm1Lex}/Mmucd) was obtained from the Mutant Mouse Regional Resource Center (University of California, Davis, CA). *Tmc1* p.D569N mice were made by Applied StemCell Inc. (Milpitas, CA) using CRISPR/Cas9 technology with a single-stranded oligonucleotide donor of the sequence given in *SI Appendix*, Fig. S1; the desired mutation was verified by 500-bp sequencing around the targeted site in F0 and in F1 pups. Mice were subsequently bred for 5 generations, after which any unlikely off-target effects should have been eliminated. *Tmc1* pM412K (*Beethoven*) mice were a gift from Karen Steel (Kings College London, UK). Both *Tmc1* M412K and *Tmc1* D569N mice were bred onto a similar CD1 background and then crossed with Tmc2$^{-/-}$. For mutants, a mixture of male and female mice was used, and no sex-specific effects were noted. Both C57Bl6 and CD1 mice were used as controls. Acoustic brainstem responses (ABRs) were measured on 4-wk-old mutant and wild-type mice of both sexes using Tucker-Davis Technology (Alachua, FL) Auditory Workstation with an RZ6 Processor equipped with BioSigRZ software. For all ABRs, mice were anesthetized with 10 mg/mL ketamine and 1 mg/mL xylazine.

Electrophysiology and Stimulation. MET currents were recorded from OHCs and inner hair cells (IHCs) in isolated organs of Corti of mice between P0 and P10 with methods described previously (10, 30). Excised cochlear turns were immobilized in a recording chamber on a fixed-stage microscope (Leica DMFS) and perfused with saline of composition (in mM): 152 NaCl, 6 KCl, 1.5 $CaCl_2$, 2 Na–pyruvate, 8 D-glucose, and 10 Na–Hepes, pH 7.4, at room temperature of 21° to 23 °C. Electrical recordings were made with patch electrodes filled with the following solution (in mM): 128 CsCl, 3.5 $MgCl_2$, 5 Na_2ATP, 10 Tris phosphocreatine, 1 BAPTA (1,2-bis(*o*-aminophenoxy)ethane-*N*,*N*,*N*′,*N*′-tetracetic acid), 10 Cs–Hepes, pH 7.2, and connected to an Axopatch 200B amplifier; recording time constants were 25 to 50 μs. Stereociliary bundles were stimulated with a fluid jet or a stiff glass probe driven by a piezoactuator and bundle displacements were calibrated (31). Single MET-channel events were characterized as previously described (12, 13). Single-channel amplitudes were also determined from MET-channel nonstationary current noise (32, 33). MET currents in response to prolonged near-maximal bundle stimuli were low-pass-filtered at 10 kHz; currents were analyzed by subtracting the mean current, I, from each of 40 or more individual traces and squaring the difference to yield the current variance, σ_I^2, which was then corrected by subtracting the variance attributable to the background noise. A plot of σ_I^2 against I was fit with the following parabolic equation: $\sigma_I^2 = i_o \cdot I - I^2/N_{MET}$, where i_o is the single-channel current and N_{MET} is the number of channels (33). The Ca^{2+} selectivity of the MET channel was determined (5, 10) by measuring the Ca^{2+} reversal potential (V_{rev}) using the following CsCl-based intracellular solution of composition (in mM): 135 CsCl, 3 MgATP, 10 Tris phosphocreatine, 1 EGTA–CsOH, 10 Hepes (pH 7.2) and an extracellular

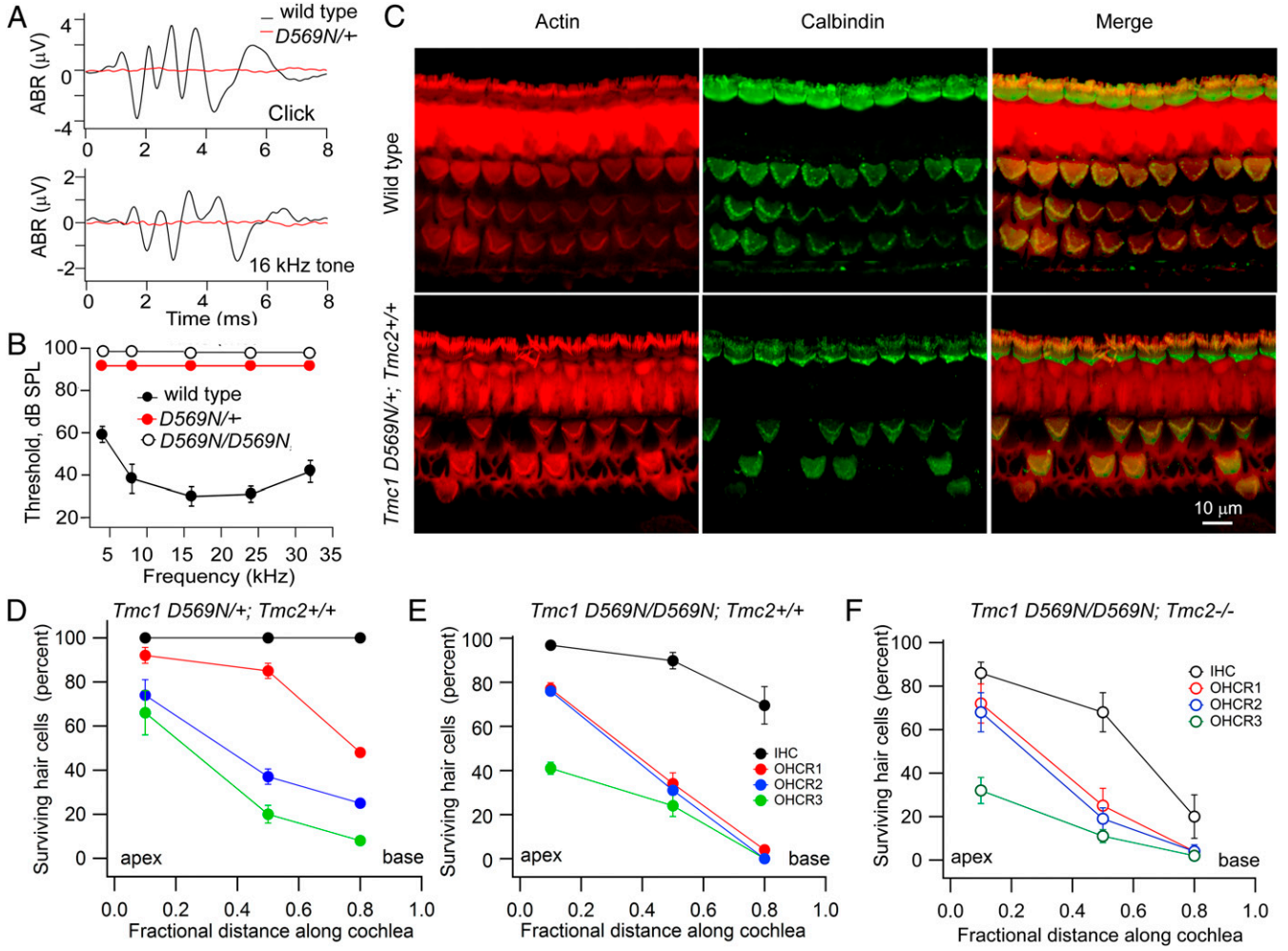

Fig. 1. Deafness and hair-cell loss in *Tmc1* p.D569N mutants. (*A*) Acoustic brainstem responses (ABRs) in P30 *Tmc1* wild-type and P30 *Tmc1* D569N/+; *Tmc2*$^{+/+}$ mice for 80-dB clicks and 80-dB 16-kHz tones. (*B*) Mean threshold for tone stimuli versus frequency in 5 wild-type mice, 4 *Tmc1* D569N/+; *Tmc2*$^{+/+}$ mice, and 3 *Tmc1* D569N/D569N; *Tmc2*$^{+/+}$ mice. For both p.D569N mutants no response was evident at 95 dB sound pressure level. (*C*) Middle turn cochleas labeled with phalloidin (red) and calbindinD-28k antibody (green) for P30 *Tmc1* wild-type (*Top*) and *Tmc1* pD569N/+; *Tmc2*$^{+/+}$ mice (*Bottom*) showing OHC loss in a heterozygote. (*D*) Surviving hair cells (percent) at 3 cochlear locations for IHC (black), and OHC stereociliary row 1 (R1, red), stereociliary row 2 (R2, blue), and stereociliary row 3 (R3, green) of P30 *Tmc1* D569N/+; *Tmc2*$^{+/+}$. (*E*) Percentage of survival at 3 cochlear locations for IHC (black), row 1 (red), row 2 (blue), and row 3 (green) OHCs of P30 *Tmc1* D569N/D569N; *Tmc2*$^{+/+}$. (*F*) Percentage of survival at 3 cochlear locations for IHC (black), and OHC stereociliary row 1 (R1, red), stereociliary row 2 (R2, blue), and stereociliary row 3 (R3, green) of P30 *Tmc1* D569N/D569N; *Tmc2-/-*. In *D*–*F*, mean ± SD of 300 cells in 3 mice.

solution (in mM): 100 $CaCl_2$, 20 *N*-methylglucamine, 6 Tris, 10 D-glucose (pH 7.4). MET current reversal potentials were corrected for a −9-mV junction potential, and the permeability ratio, P_{Ca}/P_{Cs}, was calculated from the Goldman–Hodgkin–Katz equation using activity coefficients for Cs^+ and Ca^{2+} as described previously (10).

Immunolabeling and Electron Microscopy. To document hair-cell survival in mutants, P14 and P30 cochleas were fixed in 4% paraformaldehyde for 1 h at room temperature. Cochleas were decalcified in 0.12 M EDTA in 0.1 M Na phosphate buffer at pH 7.4 for 15 to 27 h; blocked in goat serum for 1 h and immunolabeled with rabbit polyclonal anti-calbindinD28k (Swant, Bellinoza Switzerland, 1:500, 2 h), secondary Alexafluor488 antibody, and Alexa-568 phalloidin (1:500, 1 h); mounted with Fluoromount G; and viewed on an Nikon A1 confocal. TMC1 labeling was performed (15) by fixing cochleas in 4% paraformaldehyde for 10 min at room temperature and then by secondary fixation and permeabilization in an equi-volume mixture of methanol and acetone at −20 °C for 10 min, washed and labeled with TMC1 antibody (HPA 044166, Sigma Chemical Co., 1:50 dilution, for 16 h at 4 °C). Bundles were counter-labeled with espin (monoclonal anti-ESPN, BD Biosciences, 1:100 dilution). Fluorescence intensity was measured with ImageJ software. Scanning electron micrographs of cochlear hair bundles were obtained (34) using the OTOTO technique (35). Isolated cochleas were fixed in 2.5% glutaraldehyde in 0.1 M Na cacodylate buffer (pH 7.4) plus 2 mM $CaCl_2$ for 2 h, postfixed for 1 h in 1% osmium tetroxide in cacodylate buffer, washed, and incubated in a saturated filtered solution of thiocarbohydrazide for 20 min. Tissue was dehydrated through an ethanolic series, critical-point-dried from liquid CO_2, mounted, and examined in a Hitachi S-4500 field emission scanning electron microscope at 5 kV.

Results

TMC1 p.D569N Is Associated with OHC Loss and Deafness. The *Tmc1* p.D572N mutation has been reported in humans to cause dominant nonsyndromic hearing loss, but the equivalent mutation in mice has not been characterized. Acoustic brainstem responses showed that *Tmc1* p.D569N mutant mice were completely deaf by P30 (Fig. 1 *A* and *B*). At this age, there was major loss of OHCs proceeding from the base to the apex, with cell death being greater in homozygotes than in heterozygotes (Fig. 1 *C*–*E*). However, there was much smaller loss of IHCs at the same time point. OHC loss was already visible at P14, especially at the base, in *Tmc1* p.D569N/D569N homozygotes but not in *Tmc1* p.D569N/+ heterozygotes. It should be emphasized that results illustrated in Fig. 1 were for $Tmc2^{+/+}$ mice as in the human mutation, but the TMC2 isoform would have disappeared by P30, and consistent with this, the hair-cell counts were similar in the $Tmc2^{-/-}$ mutant background (Fig. 1*F*). Nevertheless, subsequent results will delineate the effects of the *Tmc1* p.D569N mutation in the presence and in the absence of TMC2. The genotypes will be referred to as *Tmc1* p.D569N/D569N; $Tmc2^{+/+}$ and *Tmc1* p.D569N/D569N; $Tmc2^{-/-}$.

The MET current in cochlear hair cells develops over the first few neonatal days and initially flows through TMC2-containing channels, but after approximately the first week, TMC2 is downregulated and the MET current is attributable to TMC1-containing channels (13). In $Tmc1^{+/+}$; $Tmc2^{-/-}$, expression of the MET channel was delayed relative to the $Tmc1^{+/+}$; $Tmc2^{+/+}$; the base of the cochlea preceded the apex by about 2 d to reach a greater maximal amplitude (Fig. 2 *A*–*C*), consistent with the tonotopic organization of the MET channel (13). Despite the profound effects on hearing in *Tmc1* p.D569N mutant mice, whether heterozygote or homozygote, OHCs still displayed MET currents during the first neonatal week. The MET channel in *Tmc1* p.D569N/D569N; $Tmc2^{-/-}$ developed over the same time period as the $Tmc1^{+/+}$; $Tmc2^{-/-}$, but reached a maximum size about one-third of the wild type at the apex (Fig. 2*C*); more importantly, there was no difference between apex and base: the OHC current amplitude at the base (P4) was not significantly different from that at the apex (P6) (2-sided *t* test, $P = 0.87$). Equivalent results were obtained from IHCs and, in the absence of TMC2, the mean current at P6 was 0.52 ± 0.01 nA ($n = 7$) in

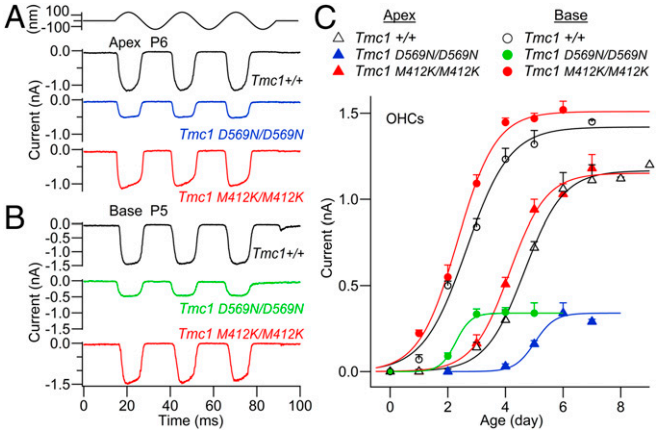

Fig. 2. MET currents in OHCs of *Tmc1* D569N; $Tmc2^{-/-}$ and *Tmc1* M412K; $Tmc2^{-/-}$ mice. (*A*) Examples of maximal MET currents in apical OHCs of $Tmc1^{+/+}$, *Tmc1* D569N/D569N, and *Tmc1* M412K/M412K at P6. (*B*) Maximal MET currents in basal OHCs of $Tmc1^{+/+}$ and *Tmc1* D569N/D569N and *Tmc1* M412K/M412K at P5. At both cochlear locations, the maximal MET current is smaller in D569N. (*C*) Development of MET current (mean ± SEM) with postnatal age. Number of OHCs with points of increasing age—$Tmc1^{+/+}Tmc2^{-/-}$: base, open circles, 4, 5, 5, 4, 4, 3; $Tmc1^{+/+}Tmc2^{-/-}$: apex, open triangles, 3, 3, 3, 5, 7, 5, 6, 3; *Tmc1* M412K/M412K; $Tmc2^{-/-}$: base, red circles, 3, 3, 4, 4, 5, 2; *Tmc1* M412K/M412K; $Tmc2^{-/-}$: apex, red triangles, 2, 5, 11, 9, 10, 6; *Tmc1* D569N/D569N; $Tmc2^{-/-}$: base, green circles, 2, 4, 5, 7, 4; and *Tmc1* D569N/D569N; $Tmc2^{-/-}$: apex, blue triangles, 3, 3, 6, 9, 5.

the $Tmc1^{+/+}$; $Tmc2^{-/-}$ and was reduced to one-third, 0.14 ± 0.01 nA ($n = 3$), in the *Tmc1* p.D569N/D569N; $Tmc2^{-/-}$ mutant. In contrast to the OHC currents in the *Tmc1* p.D569N mutant mouse, those in the *Tmc1* M412K mutant developed along a similar trajectory (although slightly earlier) to attain the same amplitude as in the wild-type mouse at both apex and base (Fig. 2*C*); indeed, even at P10 there was little reduction in MET current in *Tmc1* p.M412K/M412K; $Tmc2^{-/-}$ compared to wild-type $Tmc1^{+/+}$; $Tmc2^{-/-}$ (29). Furthermore, the *Tmc1* p.M412K accelerates expression of the MET channel relative to the *Tmc1* p.D569N. The comparison between *Tmc1* p.D569N and *Tmc1* p.M412K mutations suggests that they have different initial consequences for MET channel expression.

We also documented the effects on the MET current of the mutation on the $Tmc2^{+/+}$ wild-type background. In *Tmc1* p.D569N/D569N; $Tmc2^{+/+}$, the time course of the OHC MET current was complex, increasing to a peak and then declining (*SI Appendix*, Fig. S2). This time course reflects the initial transient expression of TMC2, followed by the appearance of the TMC1 p.D569N. The expression of the TMC1 mutant at each age was determined by subtracting the expected time course of TMC2 (13) (*SI Appendix*, Fig. S2*B*, dashed line) from that measured in *Tmc1* D569N/D569N; $Tmc2^{+/+}$ mice. The results of the subtraction are consistent with the measurements in Fig. 2*C*, confirming that there is a substantial reduction in current size in the *Tmc1* p.D569N mutant.

TMC1 Labeling and Hair Bundle Shape in the Mutant. The reduced MET current in the *Tmc1* p.D569N mutant may be caused by a diminished expression of TMC1 at the transduction site. We examined this possibility by labeling for TMC1 with an anti-TMC1 antibody (15). OHC bundles in $Tmc1^{+/+}$ showed clear labeling for the protein, but in the *Tmc1* p.D569N/D569N there was a significant reduction in the label (Fig. 3 *A* and *B*). Quantification in apical OHCs showed about a 3-fold reduction in fluorescence intensity in the mutant (Fig. 3*C*), comparable to the reduction in the OHC MET current. The hair bundle structure in OHCs was also examined in scanning electron micrographs, and

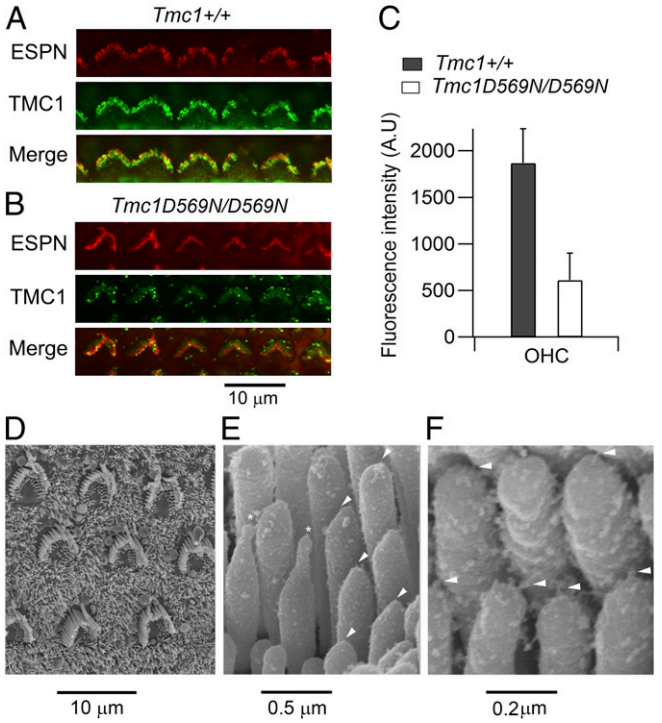

Fig. 3. TMC1 expression and OHC bundle shape in the D569N mutant. (*A*) Immunolabeling for TMC1 in the apical region of a P7 *Tmc1*$^{+/+}$; *Tmc2*$^{-/-}$ mouse cochlea. One row of OHCs is shown, the bundle structure (red fluorescence) revealed by an antibody against the actin cross-linker ESPN. (*B*) Immunolabeling in the apical region of a P7 *Tmc1* p.D569N/D569N; *Tmc2*$^{-/-}$ mouse cochlea, showing reduced TMC1 expression. (*C*) Quantification of fluorescence (mean ± SD) evaluated form 24 OHCs in each of 2 mice of each strain. TMC1 label is reduced 3.1-fold from 1,870 to 611 counts (*t* test, $P < 0.0001$). (*D*) Scanning electron micrograph of apical OHC bundles in a P7 *Tmc1* p.D569N/D569N; *Tmc2*$^{-/-}$ mouse cochlea. (*E*) Scanning electron micrograph of OHC stereocilia from P7 *Tmc1* p.D569N/D569N; *Tmc2*$^{-/-}$ mouse cochlear apex; arrowheads indicate tip links, and asterisks denote 2 distorted stereocilia with unusual elongated tips. (*F*) Higher power of OHC stereocilia in *Tmc1* p.D569N/D569N; *Tmc2*$^{-/-}$ mutant showing persistence of tip links (arrowheads).

showed a rounded U-shaped contour (Fig. 3*D*) similar to that seen in *Tmc1*$^{-/-}$; *Tmc2*$^{-/-}$ (34). There was also a distortion of the stereociliary tips (Fig. 3*E*, asterisks), as though the stereocilium had shrunk and been drawn down from its attachment point; this deformation is also prominent in *Cib2*$^{-/-}$ (18). Associated with the rounding of the OHC bundles, there was a reduction in bundle height. The height of the tallest stereociliary row, measured in isolated unfixed cochleas, was 4.3 ± 0.2 μm ($n = 9$) in *Tmc1*$^{+/+}$; *Tmc2*$^{-/-}$ and 2.8 ± 0.1 μm ($n = 11$) in *Tmc1* p.D569N/D569N; *Tmc2*$^{-/-}$, the difference being significant (*t* test, $P < 0.0001$). Despite the changes in appearance of the hair bundles and component stereocilia, there was evidence for the presence of tip links, which was unsurprising as we have previously shown the tip links to remain even in the absence of both TMC1 and TMC2 (34).

Ca^{2+} Influx in TMC1 Mutants. The amino acid D569 has been proposed from modeling to lie in the TMC1 channel pore region at the cytoplasmic face of transmembrane domain 7 (23, 24). Because of loss of the negatively charged residue, mutation at this location might affect the Ca^{2+} permeability of the MET channel. Reversal potentials for the MET current in 100 mM of extracellular Ca^{2+} saline were measured in controls and in *Tmc1* p.D569N homozygous and heterozygous mutant mice. The permeability results (Fig. 4 *A* and *B*) showed that there was a more than 3-fold reduction in Ca^{2+} permeability from $P_{Ca}/P_{Cs} = 4.20 \pm 0.7$ ($n = 10$) for the *Tmc1*$^{+/+}$; *Tmc2*$^{-/-}$ to $P_{Ca}/P_{Cs} = 1.25 \pm 0.1$ ($n = 7$) for the *Tmc1* p.D569N/D569N; *Tmc2*$^{-/-}$ homozygote; an intermediate value of $P_{Ca}/P_{Cs} = 2.11 \pm 0.5$ ($n = 6$) was measured for the *Tmc1* p.D569N/+; *Tmc2*$^{-/-}$, heterozygote. The heterozygote and homozygote were significantly different (*t* test, $p < 0.01$), as were the heterozygote and control ($P < 0.001$). Similar results were seen with the *Tmc1* p.M412K in OHCs (Fig. 4*C*), as previously reported (12, 29). The *Tmc1* p.M412K/M412K; *Tmc2*$^{-/-}$ homozygote and the *Tmc1* p.M412K/+; *Tmc2*$^{-/-}$ heterozygote were significantly different (*t* test, $P < 0.006$), as were the heterozygote and the control ($P < 0.001$). For both *Tmc1* mutants, the reduction in Ca^{2+} permeability, even in heterozygotes, may offer an explanation for the semidominance of the mutation: even with a single-mutant copy of the gene, ion conduction through the MET channel is modified. Measurements were made in *Tmc2*$^{+/+}$ mice as well as in *Tmc2*$^{-/-}$, but these 2 genotypes showed similar values (Fig. 4*C*), since at the age used (P7), the TMC2 would have almost disappeared (*SI Appendix*, Fig. S1).

Single MET Channel Currents. Another possibility is that the D569 site contributes to the conductance of cations other than Ca^{2+}. We therefore determined whether the mutation affects the single-channel conductance; this was measured in low, 0.04 mM, extracellular Ca^{2+} to maximize current amplitudes and to improve signal to noise. Single channels were isolated after brief BAPTA exposure as previously described (5, 13), the mechanical probe was moved around the bundle until isolated channels were seen, and recordings were selected in which only single-channel events were observed. The mean principal unitary current was −8.0 ± 0.4 pA based on 96 records in 3 apical OHCs (Fig. 5*A*). Of all channel events visible, this amplitude constituted 71% of all traces and was the most long-lived (Fig. 5*B*). Other brief conductance states were also seen: −4.2 pA and −11.5 pA. The distribution of event sizes accords well with that documented for

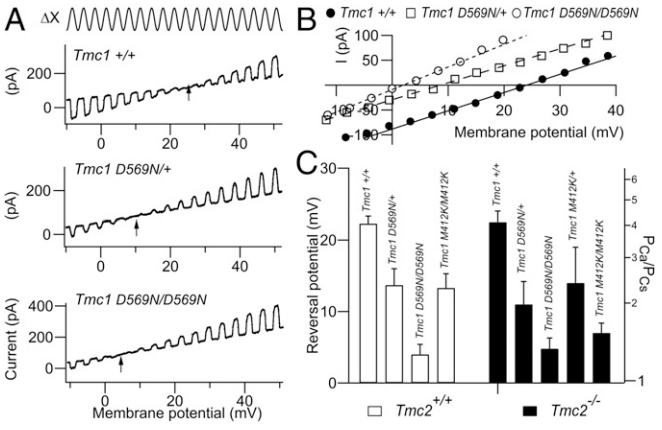

Fig. 4. MET channel Ca^{2+} permeability of apical OHCs in *Tmc1* mutants. (*A*) Ca^{2+} permeability determined from reversal potential (arrow) for continuous sinusoidal hair bundle stimulation (*Top*) during membrane potential sweeps from −50 to +50 mV: *Tmc1*$^{+/+}$; *Tmc2*$^{-/-}$; *Tmc1* pD569N/+; *Tmc2*$^{-/-}$; and *Tmc1* p.D569N/D569N; *Tmc2*$^{-/-}$ mice. Note the negative shift in reversal potential (arrows) in the mutants. (*B*) Current–voltage relationships for 3 TMC1 variants from *A*. (*C*) Collected results of reversal potential and calculated P_{Ca}/P_{Cs} (mean ± SEM) for *Tmc1*$^{+/+}$, *Tmc1* p.D569N, and *Tmc1* p.M412K in a *Tmc2*$^{+/+}$ background (open bars) and *Tmc2*$^{-/-}$ background (filled bars). Numbers of OHCs measured, from left to right—*Tmc2*$^{+/+}$: 5, 3, 6, 12 and *Tmc2*$^{-/-}$: 10, 4, 7, 10, 10. Note reduced Ca^{2+} permeability in homozygotes and intermediate reduction in heterozygotes in both mutants. All measurements on P7 mice.

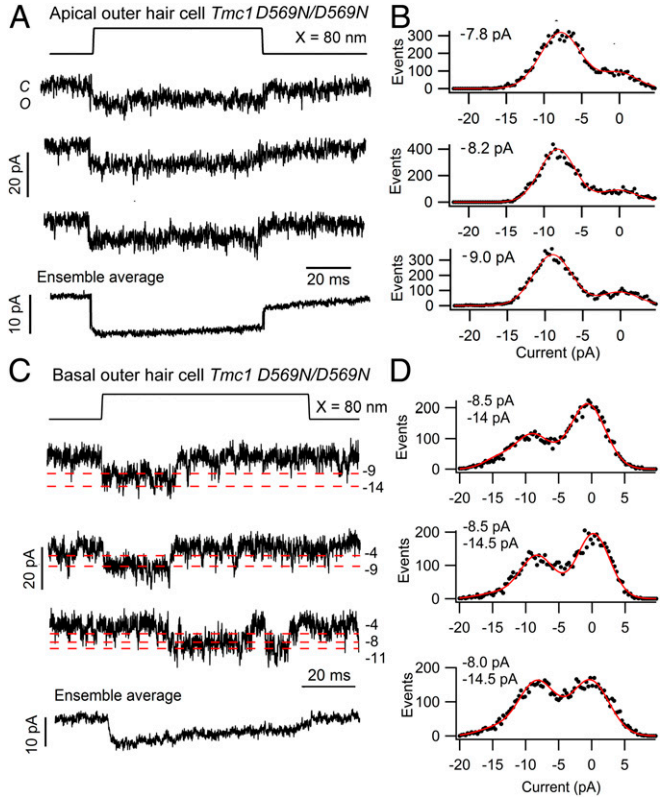

Fig. 5. Single MET channel currents in apical and basal OHCs of *Tmc1* pD569N/D569N; *Tmc2*$^{-/-}$ mice. (*A*) Three examples of single-channel records. (*Bottom*) The ensemble average current of 100 stimuli for a P5 apical OHC. (*B*) Amplitude histograms for each trace shown in *A* were fit with single Gaussians, giving channel amplitudes of −7.8, −8.2, and −9.0 pA. (*C*) Single-channel records and ensemble average of 30 presentations for a P4 basal OHC; red dashed lines indicate multiple current levels (pA). (*D*) Amplitude histograms for each trace shown in *C* were fit with single Gaussians, giving channel amplitudes of −8.5 and −14 pA; −8.5 and −14.5 pA; and −7.7 and −14.5 pA. The components at −14 or −14.5 pA were included in the fitting, but the other levels were too small to appear in the histograms. In both apical and basal hair cells, the extracellular Ca^{2+} around the bundle was 0.04 mM, and the holding potential was −84 mV.

apical OHCs from TMC1 wild-type mice (*Tmc1*$^{+/+}$; *Tmc2*$^{-/-}$) (13), indicating that the p.D569N mutation caused no reduction in the MET channel conductance. Measurements from OHCs in the *Tmc1* p.D569N/D569N; *Tmc2*$^{-/-}$ mutant at the base gave a mean principal unitary current of −7.9 ± 0.3 pA based on 100 events in 4 OHCs. Of all channel events visible, a −8 pA channel size constituted 67% of all events. Other brief conductance states were −4.0 pA, −11.0 pA, and −14.0 pA, which are evident in the recordings in Fig. 5*C*; however, in this cell the predominant level was still 8.0 to 8.5 pA (Fig. 5*D*), although the histograms all have a small −14 pA component. There were, however, no substantial large-amplitude channels as seen in controls (13). Based upon these various levels, the mean equivalent conductance G is given by the following: $G = \Sigma\,(n_i I_i)/V_H$, where I_i are the current levels and n_i are there relative proportions (13). G has a value of 95 ± 5 pS at the apex and 107 ± 6 pS at the base. While these values are different, the gradient is smaller than reported in wild type, where the base conductance is at least twice that at the apex. Measurements were also made in apical IHCs of *Tmc1* p.D569N/D569N; *Tmc2*$^{-/-}$ mutant mice (Fig. 6*B*) and gave no evidence of a reduction in the MET channel conductance in the mutant. The principal unitary current (measured in 0.04 mM external Ca^{2+}) was −7.2 ± 0.5 pA based on 60 records in 3 IHCs. As with the OHCs, there were brief additional levels at −4.2 pA, −11.3 pA, and −14.6 pA. Similar levels were seen in the control (see figure 4 of ref. 13).

Analysis of nonstationary current noise has sometimes been employed to derive the properties of a number of ion channels including the hair-cell MET channel (24, 32). We applied this technique to apical OHCs to confirm the lack of effect of the p.D569N mutation (Fig. 6*D*). The bundle displacement step was chosen so that it evoked a near maximal current but displayed adaptation, so the probability of channel opening ranged from near 0 to 1.0. Each 200-ms positive displacement of the bundle was preceded by a negative deflection to close those channels open at rest. The measurements gave similar values for the single-channel current of ∼6.0 pA in the wild type and mutant. The experiments were performed with 1.5 mM extracellular Ca^{2+} bathing the hair bundle in order to prevent run-down and optimize stationarity during prolonged data collection. Owing to Ca^{2+} block of the channel, the channel amplitude will be about 30% smaller than those in direct measurements of single-channel

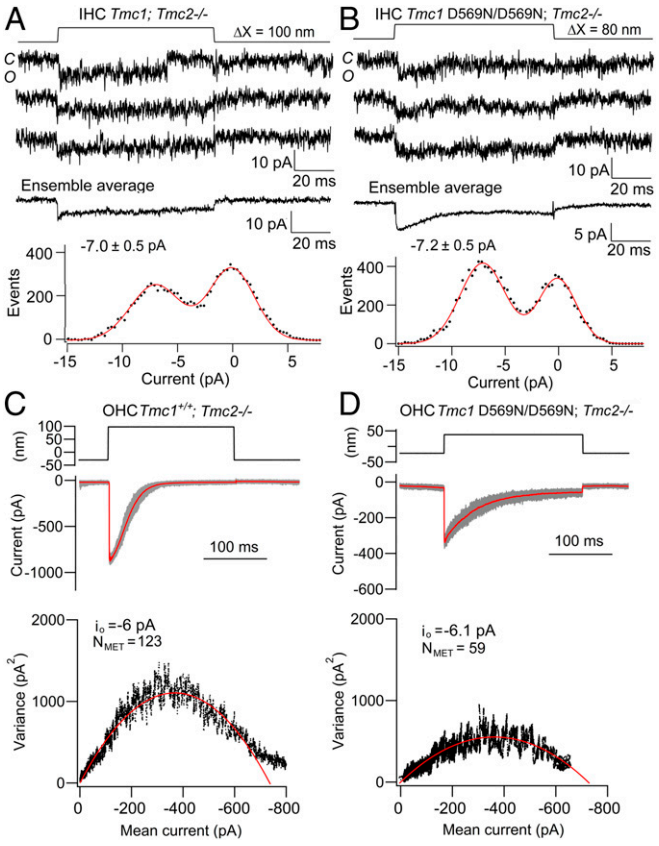

Fig. 6. Single MET channel current amplitudes are unaltered in hair cells of *Tmc1* p.D569N/D569N mice. (*A*) Single-channel records in the *Tmc1*$^{+/+}$; *Tmc2*$^{-/-}$ mouse, ensemble average of 40 stimuli, and amplitude histogram with channel of −6.9 pA. (*B*) Single-channel records, ensemble average of 100 presentations, and amplitude histogram of *Tmc1* p.D569N/D569N; *Tmc2*$^{-/-}$ with channel of −7.1 pA. *A* and *B* are for P6 mouse apical IHCs. (*C*) OHC MET currents in the *Tmc1*$^{+/+}$; *Tmc2*$^{-/-}$ mouse with mean current (red) with individual responses (gray) for 50 stimuli superimposed. (*Bottom*) Plot of current variance σ_i^2 versus current amplitude I, fit with parabolic equation (*Materials and Methods*) giving single-channel current i_o = −6.0 pA and number of channels N_{MET} = 123. (*D*) OHC MET currents in *Tmc1* p.D569N/D569N; *Tmc2*$^{-/-}$ mouse with mean current (red) with individual responses (gray) for 40 stimuli superimposed. (*Bottom*) Plot of current variance σ_i^2 versus current I, gives i_o = −6.1 pA) and N_{MET} = 59. *C* and *D* are for P6 mouse apical OHCs; extracellular Ca^{2+} was 0.04 mM (*A* and *B*) and 1.5 mM (*C* and *D*).

events, all of which were done in 0.04 mM Ca^{2+}. For apical OHCs, the mean unitary current (±SD) inferred from the noise analysis was −6.5 ± 1.2 pA (n = 6) for *Tmc1*$^{+/+}$; *Tmc2*$^{-/-}$ and 6.0 ± 0.8 pA (n = 7) for *Tmc1* p.D569N/D569N; *Tmc2*$^{-/-}$. There was no significant difference between these current amplitudes (t test, $P = 0.3$). The analysis also yielded the number of channels per cell: 185 ± 40 channels for the *Tmc1*$^{+/+}$; *Tmc2*$^{-/-}$ control and 62 ± 20 for the *Tmc1* p.D569N/D569N; *Tmc2*$^{-/-}$. The result supports the conclusion that the D569N mutation substantially reduces channel expression, as found with the macroscopic current, without a change in channel conductance (Fig. 2).

Discussion

Our study highlights possible mechanisms for the autosomal dominant human deafness DFNA36 caused by the single-amino-acid substitution D572N (7) (equivalent to D569N in mice). It should be emphasized that the acoustic brainstem responses and hair-cell counts (Fig. 1) were done on a *Tmc2*$^{+/+}$ background as appropriate for comparison with the human mutation. However, hair-cell recordings could be made only before about P9, so most measurements of current amplitude (Fig. 2) and single-channel recordings (Figs. 5 and 6) were performed on a *Tmc2*$^{-/-}$ background to circumvent contamination from TMC2-containing MET channels, which are down-regulated after P8. Nevertheless, the main conclusions were verified by some results with TMC2 present (*SI Appendix*, Fig. S1). Moreover, the effects on channel Ca^{2+} permeability were documented in the presence and absence of TMC2 (Fig. 4*C*).

According to recent modeling (23, 24), the D572 site could lie near the cytoplasmic end of the ion-conducting cavity of a hypothetical channel formed by TMC1. The mouse mutational deficits fall into 2 categories: those similar to *Tmc1* p.M412K and those unique to *Tmc1* p.D569N. The former category includes decreased Ca^{2+} permeability, misshapen hair bundles, and ultimately OHC apoptosis proceeding from base to apex. Some of these have been reported previously for *Tmc1* p.M412K (11, 12, 28, 29, 36). The latter category unique to *Tmc1* p.D569N is a substantial reduction in the maximum MET current and loss of its tonotopic gradient in OHCs. Thus, the p.D569N mutation may affect the expression and trafficking of the MET channel, possibly by impaired interaction of TMC1 with other constituents of the mechanotransduction complex, whereas the p.M412K mutation does not. Reduction in the maximum current in *Tmc1* p.D569N (but not in *Tmc1* p.M412K) (12) will further diminish the influx of Ca^{2+}, which could be a key change ultimately triggering cell death. With regard to the misshapen or U-shaped hair bundles and reduced bundle height, one hypothesis is that the hair bundle, which matures over the first neonatal week, may require Ca^{2+} influx to preserve actin polymerization and also the shape of the top of the OHC and cuticular plate. Ca^{2+} influx is likely to be reduced in *Tmc1*$^{-/-}$; *Tmc2*$^{-/-}$ and *Cib2*$^{-/-}$ where there is no normal MET current (18, 30) and in both *Tmc1* mutations described here. It is noteworthy that some protection is afforded by the early presence of TMC2, which will permit Ca^{2+} to enter the cell over the first postnatal week. Ca^{2+} influx via the MET channels has been shown to be essential for maintaining stereociliary structure and the stability of the cytoskeleton (37). Despite the reduction in Ca^{2+} permeability associated with the *Tmc1* p.D569N and *Tmc1* p.M412K mutations, the lack of change in channel conductance in either mutant raises the concern that TMC1 does not on its own form the pore. Other contributors may include TMIE (16, 17) and CIB2 (18), as well as currently unidentified components. For the OHCs, we previously concluded that the tonotopic size gradient reflects differential expression of TMC1 molecules at the transduction site, with more molecules at the base than at the apex (13). The absence of a OHC tonotopic gradient in the *Tmc1* p.D569N may partly reflect an overall reduction in the number of TMC1 molecules at the transduction site at both apex and base, rather than any change in the unitary conductance of individual subunits. No such reduction in TMC1 expression is expected for *Tmc1* p.M412K (Fig. 1*C*), and the tonotopic gradient in channel conductance persists (12).

An important unanswered question is why the p.D569N mutation causes hair-cell death and deafness. Is it a direct consequence of the reduced Ca^{2+} influx, linked to downstream signaling via, for example, a Ca^{2+}/calmodulin-stimulated protein kinase? Features of hair-cell death in this circumstance, as with gentamicin toxicity, are its delayed onset (38) and progression in OHCs from cochlear base to apex (39). Our results demonstrate a major difference between the effects of the 2 mutants, p.D569N and p.M412K, with reduction in the MET current and loss of tonotopy in the former but not in the latter. Nevertheless, both mutations show hair-cell loss by P30 (36) [although, curiously, the relative loss of IHCs and OHCs in *Tmc1* p.M412K depends on background strain (40)]. It is possible that the *Tmc1* p.D569N channel is less stable than the *Tmc1* M412K, thus accounting for the reduction in current, but that alone cannot explain the hair-cell death. It is also conceivable that TMC1 has some other regulatory effect perhaps linked to reduced Ca^{2+} influx in the endoplasmic reticulum (22), and it is this aspect which is disrupted in both mutants. Thus protein synthesis, folding, and quality control may all be modulated by Ca^{2+} in the endoplasmic reticulum lumen (41). Such a regulatory role of TMC1 was implied by its effect on development and sexual behavior in the worm (42), and the topic will be worth future study to fully elucidate the various roles of TMC1.

ACKNOWLEDGMENTS. This work was funded by National Institute on Deafness and other Communication Disorders Grants RO1 DC015439 and RO1 DC01362 (to R.F.). We thank Donata Oertel and Cyndie Chow for advice with the ABR machine and the University of Wisconsin Biochemistry Optical Core for use of the Nikon A1 confocal microscope.

1. J. A. Assad, G. M. Shepherd, D. P. Corey, Tip-link integrity and mechanical transduction in vertebrate hair cells. *Neuron* **7**, 985–994 (1991).
2. M. Beurg, R. Fettiplace, J. H. Nam, A. J. Ricci, Localization of inner hair cell mechanotransducer channels using high-speed calcium imaging. *Nat. Neurosci.* **12**, 553–558 (2009).
3. S. Mahendrasingam, D. N. Furness, Ultrastructural localization of the likely mechanoelectrical transduction channel protein, transmembrane-like channel 1 (TMC1) during development of cochlear hair cells. *Sci. Rep.* **9**, 1274 (2019).
4. H. Ohmori, Mechano-electrical transduction currents in isolated vestibular hair cells of the chick. *J. Physiol.* **359**, 189–217 (1985).
5. M. Beurg, M. G. Evans, C. M. Hackney, R. Fettiplace, A large-conductance calcium-selective mechanotransducer channel in mammalian cochlear hair cells. *J. Neurosci.* **26**, 10992–11000 (2006).
6. R. Fettiplace, K. X. Kim, The physiology of mechanoelectrical transduction channels in hearing. *Physiol. Rev.* **94**, 951–986 (2014).
7. K. Kurima *et al.*, Dominant and recessive deafness caused by mutations of a novel gene, TMC1, required for cochlear hair-cell function. *Nat. Genet.* **30**, 277–284 (2002).
8. Y. Kawashima *et al.*, Mechanotransduction in mouse inner ear hair cells requires transmembrane channel-like genes. *J. Clin. Invest.* **121**, 4796–4809 (2011).
9. K. Kurima *et al.*, TMC1 and TMC2 localize at the site of mechanotransduction in mammalian inner ear hair cell stereocilia. *Cell Rep.* **12**, 1606–1617 (2015).
10. K. X. Kim, R. Fettiplace, Developmental changes in the cochlear hair cell mechanotransducer channel and their regulation by transmembrane channel-like proteins. *J. Gen. Physiol.* **141**, 141–148 (2013).
11. B. Pan *et al.*, TMC1 and TMC2 are components of the mechanotransduction channel in hair cells of the mammalian inner ear. *Neuron* **79**, 504–515 (2013).
12. M. Beurg, A. C. Goldring, R. Fettiplace, The effects of Tmc1 Beethoven mutation on mechanotransducer channel function in cochlear hair cells. *J. Gen. Physiol.* **146**, 233–243 (2015).
13. M. Beurg *et al.*, Variable number of TMC1-dependent mechanotransducer channels underlie tonotopic conductance gradients in the cochlea. *Nat. Commun.* **9**, 2185 (2018).
14. W. Xiong *et al.*, TMHS is an integral component of the mechanotransduction machinery of cochlear hair cells. *Cell* **151**, 1283–1295 (2012).
15. M. Beurg, W. Xiong, B. Zhao, U. Müller, R. Fettiplace, Subunit determination of the conductance of hair-cell mechanotransducer channels. *Proc. Natl. Acad. Sci. U.S.A.* **112**, 1589–1594 (2015).

16. B. Zhao *et al*., TMIE is an essential component of the mechanotransduction machinery of cochlear hair cells. *Neuron* **84**, 954–967 (2014).
17. I. V. Pacentine, T. Nicolson, Subunits of the mechano-electrical transduction channel, Tmc1/2b, require Tmie to localize in zebrafish sensory hair cells. *PLoS Genet.* **15**, e1007635 (2019).
18. A. P. J. Giese *et al*., CIB2 interacts with TMC1 and TMC2 and is essential for mechanotransduction in auditory hair cells. *Nat. Commun.* **8**, 43 (2017).
19. V. Labay, R. M. Weichert, T. Makishima, A. J. Griffith, Topology of transmembrane channel-like gene 1 protein. *Biochemistry* **49**, 8592–8598 (2010).
20. W. T. Harkcom, M. Papanikolaou, V. Kanda, S. M. Crump, G. W. Abbott, KCNQ1 rescues TMC1 plasma membrane expression but not mechanosensitive channel activity. *J. Cell. Physiol.* **234**, 13361–13369 (2019).
21. Y. Hahn, D. S. Kim, I. H. Pastan, B. Lee, Anoctamin and transmembrane channel-like proteins are evolutionarily related. *Int. J. Mol. Med.* **24**, 51–55 (2009).
22. L. Sirianant, J. Ousingsawat, Y. Tian, R. Schreiber, K. Kunzelmann, TMC8 (EVER2) attenuates intracellular signaling by Zn2+ and Ca2+ and suppresses activation of Cl- currents. *Cell. Signal.* **26**, 2826–2833 (2014).
23. A. Ballesteros, C. Fenollar-Ferrer, K. J. Swartz, Structural relationship between the putative hair cell mechanotransduction channel TMC1 and TMEM16 proteins. *eLife* **7**, e38433 (2018).
24. B. Pan *et al*., TMC1 forms the pore of mechanosensory transduction channels in vertebrate inner ear hair cells. *Neuron* **99**, 736–753.e6 (2018).
25. S. Kitajiri, T. Makishima, T. B. Friedman, A. J. Griffith, A novel mutation at the DFNA36 hearing loss locus reveals a critical function and potential genotype-phenotype correlation for amino acid-572 of TMC1. *Clin. Genet.* **71**, 148–152 (2007).
26. Y. Zhao *et al*., A novel DFNA36 mutation in TMC1 orthologous to the Beethoven (Bth) mouse associated with autosomal dominant hearing loss in a Chinese family. *PLoS One* **9**, e97064 (2014).
27. T. Yang *et al*., A novel mutation adjacent to the Bth mouse mutation in the TMC1 gene makes this mouse an excellent model of human deafness at the DFNA36 locus. *Clin. Genet.* **77**, 395–398 (2010).
28. S. Vreugde *et al*., Beethoven, a mouse model for dominant, progressive hearing loss DFNA36. *Nat. Genet.* **30**, 257–258 (2002).
29. L. F. Corns, S. L. Johnson, C. J. Kros, W. Marcotti, Tmc1 point mutation affects Ca2+ sensitivity and block by dihydrostreptomycin of the mechanoelectrical transducer current of mouse outer hair cells. *J. Neurosci.* **36**, 336–349 (2016).
30. M. Beurg, K. X. Kim, R. Fettiplace, Conductance and block of hair-cell mechanotransducer channels in transmembrane channel-like protein mutants. *J. Gen. Physiol.* **144**, 55–69 (2014).
31. A. C. Crawford, R. Fettiplace, The mechanical properties of ciliary bundles of turtle cochlear hair cells. *J. Physiol.* **364**, 359–379 (1985).
32. T. Holton, A. J. Hudspeth, The transduction channel of hair cells from the bull-frog characterized by noise analysis. *J. Physiol.* **375**, 195–227 (1986).
33. E. Neher, C. F. Stevens, Conductance fluctuations and ionic pores in membranes. *Annu. Rev. Biophys. Bioeng.* **6**, 345–381 (1977).
34. K. X. Kim *et al*., The role of transmembrane channel-like proteins in the operation of hair cell mechanotransducer channels. *J. Gen. Physiol.* **142**, 493–505 (2013).
35. D. N. Furness, C. M. Hackney, High-resolution scanning-electron microscopy of stereocilia using the osmium-thiocarbohydrazide coating technique. *Hear. Res.* **21**, 243–249 (1986).
36. W. Marcotti, A. Erven, S. L. Johnson, K. P. Steel, C. J. Kros, Tmc1 is necessary for normal functional maturation and survival of inner and outer hair cells in the mouse cochlea. *J. Physiol.* **574**, 677–698 (2006).
37. A. C. Vélez-Ortega, M. J. Freeman, A. A. Indzhykulian, J. M. Grossheim, G. I. Frolenkov, Mechanotransduction current is essential for stability of the transducing stereocilia in mammalian auditory hair cells. *eLife* **6**, e24661 (2017).
38. Y. J. Kim *et al*., Autophagic flux, a possible mechanism for delayed gentamicin-induced ototoxicity. *Sci. Rep.* **7**, 41356 (2017).
39. R. Fettiplace, J. H. Nam, Tonotopy in calcium homeostasis and vulnerability of cochlear hair cells. *Hear. Res.* **376**, 11–21 (2019).
40. Y. Noguchi *et al*., Multiple quantitative trait loci modify cochlear hair cell degeneration in the Beethoven (Tmc1Bth) mouse model of progressive hearing loss DFNA36. *Genetics* **173**, 2111–2119 (2006).
41. J. Krebs, L. B. Agellon, M. Michalak, Ca(2+) homeostasis and endoplasmic reticulum (ER) stress: An integrated view of calcium signaling. *Biochem. Biophys. Res. Commun.* **460**, 114–121 (2015).
42. L. Zhang *et al*., TMC-1 attenuates C. elegans development and sexual behaviour in a chemically defined food environment. *Nat. Commun.* **6**, 6345 (2015).